



An Experimental Verification of Iterative Microphone Removal Beamforming Arrays

Elias Arcondoulis, Pengwei Xu and Yu Liu

Department of Mechanics and Aerospace Engineering, Southern University of Science and Technology, Shenzhen, China.

ABSTRACT

Acoustic beamforming is an experimental method that is used to locate and quantify acoustic sources and is becoming increasingly popular as a research tool in academia and a competitive edge for acoustic consultants. A microphone array design method previously presented by the current authors is experimentally verified in this paper. Based on main lobe width and maximum sidelobe criteria, an array is designed such that microphones are removed from a large array stencil to arrive at a least-compromised array design. This paper presents new arrays possessing 48-channels that are designed specifically for individual frequencies and are installed within a 169-channel stencil. For each beamforming frequency of interest, the microphones are rearranged using an iterative microphone removal method to develop a well-designed array for that frequency. Eight 48-channel arrays are designed, experimentally tested and compared with expected numerical beamforming maps. Good agreement is achieved considering the reflective properties of the testing environment and size of the acoustic source.

1 INTRODUCTION

Aeroacoustic beamforming is an application of phased array technology that has been used successfully for the study of airfoil trailing edge noise (Brooks and Humphreys, 2006) and aircraft landing gear (Dobrzynski et al., 2010). The principles of array design have been of interest since the inception of acoustic beamforming, with many improvements of beamformer array output and attempts at optimisation. Logarithmic spiral array patterns have been shown to produce efficient array patterns for a given number of microphones and allowable array area (Dougherty, 1998; Underbrink, 2002; Arcondoulis et al., 2011; Prime and Doolan, 2013) yet customising an array for a specific frequency range and for sources that may exist away from the scanning grid origin is difficult. A logarithmic array design may not be interchangeable and is typically designed for general use over a range of frequencies and source locations. Most recently, deep learning algorithms utilising neural networks have been used to resolve acoustic sources with very high speed computation compared to DAMAS (Brooks and Humphreys, 2006) and other post-processing methods (Ma and Liu, 2018). Efforts have been made to optimise array designs by using cost functions to minimise the Maximum Sidelobe Level (MSL) (Sijtsma, 1997 & 2010; Malgoezar et al., 2016; Bjelić et al., 2017) that yield significant improvements of MSL relative to an initial array design yet none of these designs conclusively display a superior combination of MSL and Main Lobe Width (MLW) compared to logarithmic spiral arrays and their variations. Luesutthiviboon et al. (2018) used an optimization algorithm aiming at simultaneously reducing MSL and MLW and presented some small performance improvements relative to an Underbrink (2002) spiral of similar dimensions.

Arcondoulis and Liu (2018) recently presented a unique algorithm that iteratively removes microphones from an existing array possessing many more microphones than the desired array based on sidelobe and main lobe criteria. The microphone that produces the smallest product of frequency-averaged MSL and MLW of the beamformer response when shaded "off" is detected using cross-spectral beamforming (Brooks and Humphreys, 2006). This microphone is then removed and this process is repeated until the predetermined desired number of microphones is reached. The benefits of this array design method is that many arrays can be designed within a stencil for varying source locations and frequencies of interest. In this paper, this iterative microphone removal method is applied to acoustic sources of single frequency (1 kHz, 2 kHz and 5 kHz) and white noise (tested at 2 kHz, 4 kHz and 6 kHz). Arrays possessing 48-channels are specifically designed for sources at the scanning grid origin and also offset 200 mm (20% of the scanning grid length) from the origin. These arrays are experimentally tested in an office-like environment that show good agreement with the numerical beamformer source maps.

2 CONVENTIONAL BEAMFORMING METHOD

In order to design the array and conduct numerical simulations, a spherical wave source (i.e., a monopole source) of unit source strength in still conditions is simulated. The propagation of this wave to the array plane can be represented as p represents a vector of complex pressures (Pa) in the frequency domain ($M \times 1$), defined as

$$p = \frac{1}{4\pi r_s} \exp\left[\frac{-j2\pi f r_s}{c}\right] \quad (1)$$

where f represents frequency (Hz), c is the speed of sound in air (343 m/s) and the variable m denotes a microphone number and ranges from 1 to M , where M is the number of microphones in the array. The distances from the source point to the microphones are given by r_s .

The cross-spectral beamforming algorithm (Brooks and Humphreys, 2006) require a complex pressure magnitude and phase at each microphone. This data is processed first in the beamforming algorithm, in a cross-spectral matrix (C) defined as

$$C = pp^T \quad (2)$$

where p represents a vector of complex pressures for each microphone and T represents the complex transpose and conjugate. The diagonal entries are set to zero to remove the autospectra from the matrix (Humphreys and Brooks, 1998).

A beamforming output is computed over a square-planar discretised grid of N data points (scanning grid) at a known distance from the array, positioned in line with the centre of the microphone array. Steering vectors, \hat{v} , contain the unique distances of each scanning grid point to each microphone, m . The steering vector for the m_{th} microphone is a $N \times 1$ array defined as

$$v = \frac{1}{4\pi r_m} \exp\left[\frac{-j2\pi f r_m}{c}\right] \quad (3)$$

$$\hat{v} = [v(1) \ v(2) \ \dots \ v(M)] \quad (4)$$

where r_m is the vector between the scanning grid point to the microphone m . The cross-spectral beamforming output, Y (Brooks and Humphreys, 2006) is computed using

$$Y(\hat{v}) = \frac{\hat{v}^T \{w C w^T\} \hat{v}}{(\sum_{m=1}^M w)^2 - (\sum_{m=1}^M w)} \quad (5)$$

where w represents the $1 \times M$ microphone shading vector. The shading quantity adjusts the microphone pressures relative to each other. In this study, values of w are either 0 or 1 to simulate a microphone being removed or included in the array respectively.

3 ARRAY SIMULATION AND DESIGNS

The iterative microphone removal method presented in a recent publication by Arcondoulis and Liu (2018) is used here to design arrays for varying frequencies and expected source locations. This method involves simulating a large initial grid array of microphones with a monopole source at a known location and distance from the array. By shading microphones "off" one-at-a-time, the microphone that results in the least impact of the product of MSL and MLW (defined as Φ) when shaded off, is removed from the array stencil. This process is repeated until the desired number of microphones remains. The definitions of MSL, MLW and Φ in this paper are

$$\text{MSL (dB)} = 20 \log_{10} \left\{ \frac{Y_s}{Y_{\max}} \right\} \quad (6)$$

$$\text{MLW (\%)} = 100 \times \left\{ \frac{N_{3\text{dB}}}{N} \right\} \quad (7)$$

$$\Phi \text{ (dB)} = 10 \log_{10} \left\{ \frac{Y_s}{Y_{\max}} \times \frac{N_{3\text{dB}}}{N} \right\} + 20 \quad (8)$$

where Y_{\max} is the main lobe amplitude (Pa) and $N_{3\text{dB}}$ is the number of scanning grid points that are occupied by the main lobe from its peak ($Y_{\max} = 0$ dB) to -3 dB. In the case of multi-frequency array design, Φ is replaced with Φ_{av} which is simply the average of the MSL and MLW the beamforming frequencies, f_s , considered. The expression for Φ_{av} is defined as

$$\Phi_{\text{av}} \text{ (dB)} = 10 \log_{10} \left(\frac{1}{f_s} \sum_1^{f_s} \left\{ \frac{Y_s}{Y_{\max}} \times \frac{N_{3\text{dB}}}{N} \right\} \right) + 20 \quad (9)$$

3.1 Initial Array Stencil

A 169-channel initial array stencil is designed using a power-relationship with respect to linear spacing, as introduced in Arcondoulis and Liu (2018). The initial array stencil spans an area of 1000 mm \times 1000 mm and has non-equispaced microphone locations. The minimum spacing of the microphones in this array is approximately 34 mm. This leaves sufficient clearance for safely and conveniently adding and removing microphones from the array. The array stencil is presented in Figure 1(a).

Small positioning errors (human error) occurred when the array grid locations were drilled into the Medium Density Fibreboard (MDF) panel, as presented in Section 4, Figure 2. These errors were quantified and incorporated into the initial array stencil prior to conducting the array reduction method (i.e., the array was designed based on an imperfect grid so that the numerical and physical array coordinates were the same).

3.2 Simulation Conditions

Two source locations were considered: the scanning grid origin $x,y = [0,0]$ (mm) and an offset location $x,y = [200,0]$ (mm). For the single-frequency arrays, the beamformer response to a monopole source, Y , is computed at $f_s = 1$ frequency (e.g., $f_{\min} = f_{\max} = 1$ kHz) over a 1000 mm \times 1000 mm scanning grid comprised of $N = 51 \times 51 = 2601$ scanning grid points. For the multi-frequency arrays, the beamformer response to a monopole source, Y , is computed at $f_s = 10$ frequencies equispaced between $f_{\min} = 2$ kHz and $f_{\max} = 8$ kHz over the same scanning grid as the single-frequency simulations. This scanning grid used to design the arrays is relatively coarse to significantly reduce the overall array reduction computation time. The array performance, once it is designed, is calculated over a more refined scanning grid of $N = 101 \times 101 = 10,201$ scanning grid points.

3.3 Example Array Simulation

An example array simulation is presented in Figure 1. This figure reveals the initial array stencil of 169-channels in a non-equispaced grid that includes the human errors during the MDF drilling process (Figure 1(a)) and the systematic removal of microphones from 169-channels to 48-channels (Figures 1(b) through 1(g)). Figure 1(h) displays the evolution of the MSL and MLW with microphone removal. The MSL and MLW values are presented in dB, normalised to the 169-channel values. It can be observed that MLW actually improves as the simulation progresses. Furthermore, the microphone removal causes a net decrease in MSL. This is due to the grating lobes that are always present with equispaced (or near equispaced) grid arrays (Sijtsma, 1997). By removing a significant portion of the grid array, the number of redundant microphone spacings that comprise the grid structure are reduced thus minimising the grating lobe magnitudes. By retaining the microphones near the array area boundaries, the MLW performance of a 1 kHz beamformer map is maintained with microphone removal, as low frequency MLW values are dictated by microphones separated by large spacings. To assist the visualisation of the start and end points of the simulation, Figures 1(i) and 1(j) reveal the beamformer maps of the 1 kHz source located at the scanning grid origin for the 169-channel and 48-channel arrays, respectively. It can be seen that the 48-channel main lobe (within a -15 dB range) is slightly smaller in diameter than the 169-channel array. The difference in sidelobes cannot be observed by comparing these two figures, as the MSL for both arrays is less than -30 dB relative to the main lobe amplitude.

4 EXPERIMENTAL PROCEDURES

In the absence of an anechoic facility, tests were conducted in an office-like environment as shown in Figure 2. Efforts were made to minimise any reflective sources by covering regions of the floor and behind the speaker source with polyurethane foam blocks. The array and speaker configuration were located in a room corner, as this was the only space available to conduct the tests. The untreated room is approximately 8 m \times 6 m.

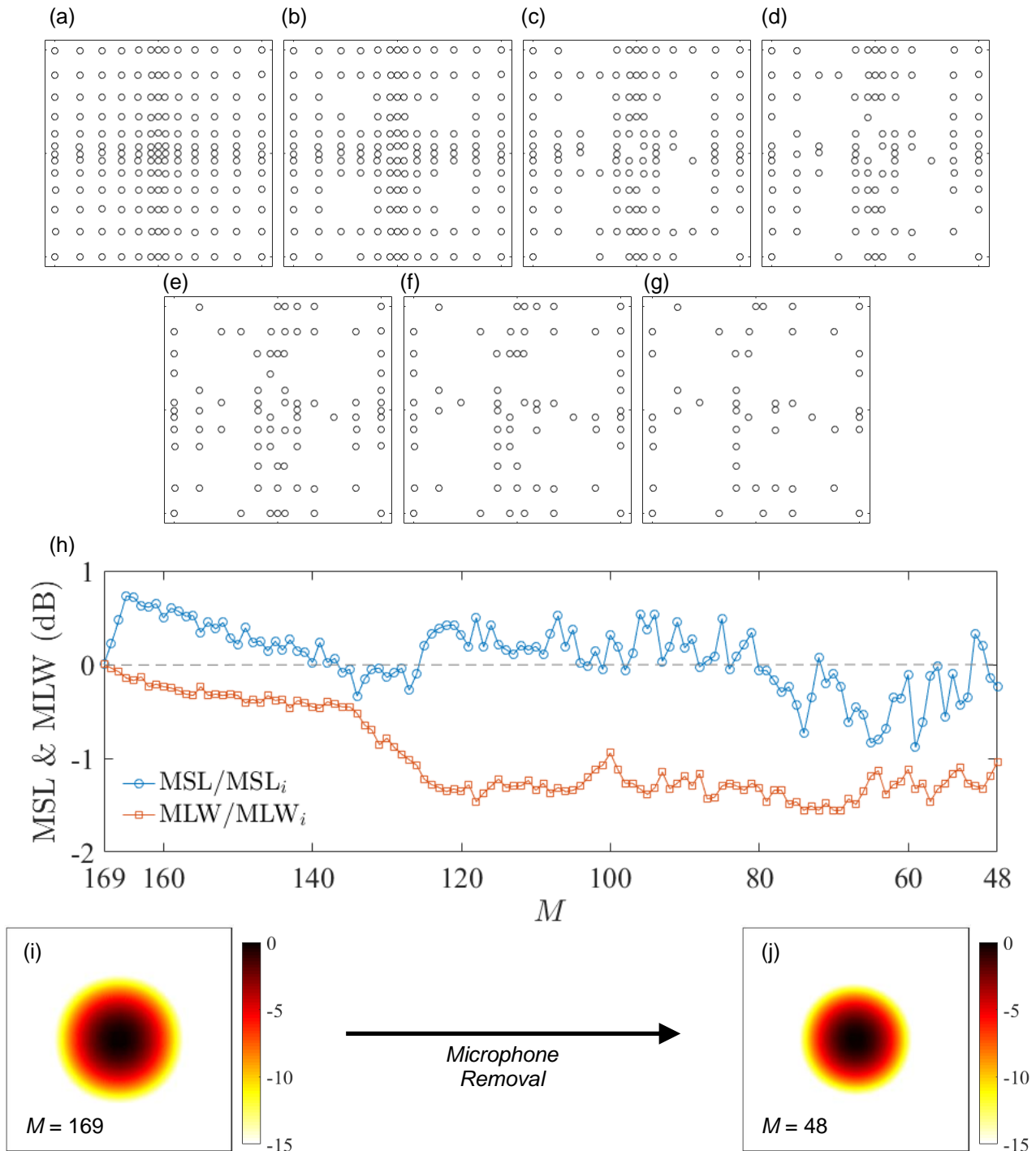


Figure 1: Various stages of a one-by-one array reduction method: from a non-equispaced 169-channel grid array to an $f = 1$ kHz centre-designed 48-channel array. Progress arrays contained within a 1000 mm \times 1000 mm area (a) 169-channels (b) 150-channels (c) 120-channels (d) 100-channels (e) 80-channels (f) 64-channels and (g) final 48-channel array. Figure (h) reveals the evolution of the normalised MSL and MLW (with respect to the initial 169-channel MSL and MLW) with reducing number of microphones. Figures (i) and (j) represent the 169-channel and 48-channel cross-spectral beamforming maps respectively.

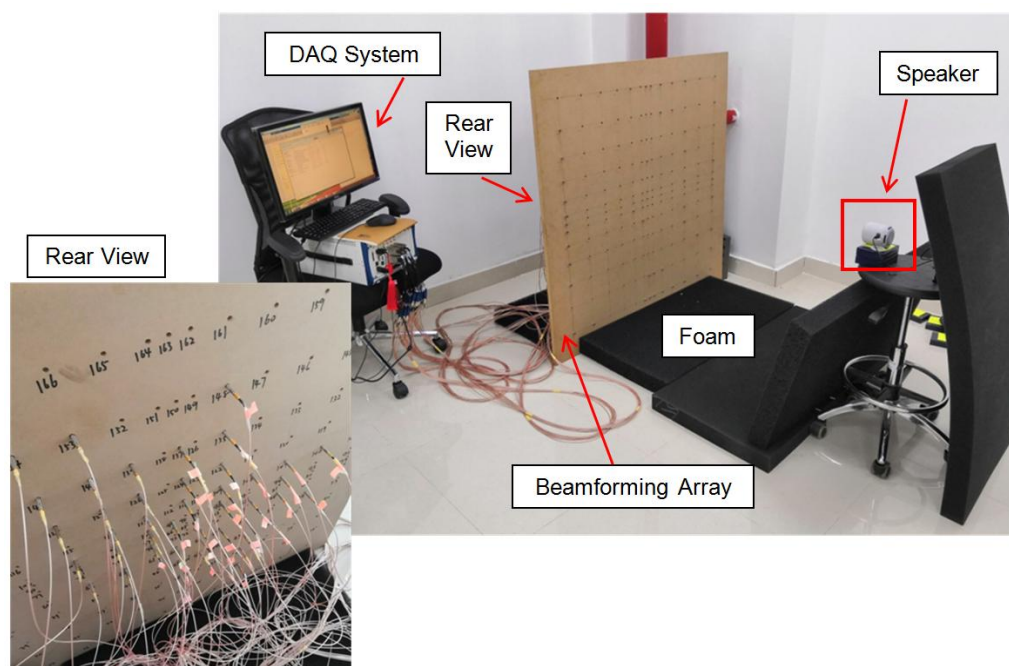


Figure 2: Experimental set-up identifying the beamforming array configuration. The image to the left shows part of the numbered array stencil used to locate the required microphones of the 48-channel array.

A 1200 mm × 1200 mm × 20 mm MDF panel was used to contain the 1000 mm × 1000 mm array stencil. BSWA MPA426 1/4" array microphones were used for the array designs presented in Section 5. Each of the microphones were calibrated using a 1 kHz piston-phone calibrator. Microphones were interchanged into the holes drilled into the rear of the MDF panel based on the arrays designed using the method detailed in Section 3. The speaker shown in Figure 2 is a SONY SRS-XB10, which has a cone diameter of approximately 50 mm. Tonal and broadband noise sources were played through the speaker using a Smartphone via Bluetooth connectivity at the two locations introduced in Section 3.2. The tonal noise frequencies used in this study are 1 kHz, 2 kHz and 5 kHz to match the frequencies used to design the single-frequency arrays presented in Section 5. A white noise signal was also used to test the multi-frequency arrays. Due to the suspected limited frequency range of the speaker, only frequencies less than or equal to 6 kHz are considered for the multi-frequency array. The data acquisition (DAQ) system used for this study consists of a National Instruments (NI) PXI-1042Q Chassis, with three PXI-4496 DAQ cards. Each card is capable of storing 16 channels of data, thus allowing up to 48 channels of real-time data. A MATLAB DAQ interface was used to collect these data, which were then run through a Fast Fourier Transform (FFT) to convert the data into the frequency domain. The data were acquired at a sampling frequency of 32,768 Hz (2^{15} Hz) for 16 seconds and then band-pass filtered between 50 Hz and at $2^{15} / 2.2 \approx 15$ kHz.

5 RESULTS

The results presented in this section are cross-spectral beamformer outputs, Y , calculated over a 1000 mm × 1000 mm scanning grid located 1000 mm from the array. The dB scale in the figures is Y / Y_{\max} . The MLW values displayed within the beamformer maps are calculated using -3 dB and -15 dB thresholds from Y_{\max} . The array bounding boxes span a 1000 mm × 1000 mm area. The results are divided into two sections: the arrays that are designed using a source located at the scanning grid origin (referred herein as Centred Design Arrays) and the arrays that are designed using a source located offset from the scanning grid origin (referred herein as Non-Centred Design Arrays).

5.1 Centred Design Arrays

Figures 3(a), 3(d) and 3(g) reveal the arrays that are designed using the iterative microphone removal method detailed in Section 3 based on an expected acoustic at the scanning grid origin ($x = y = 0$ mm) for single-frequencies 1 kHz, 2 kHz and 5 kHz, respectively. It can be observed that with increasing frequency, the microphones cluster further towards the array geometric centre with smaller microphone spacings. This is consistent

with logarithmic spiral arrays designs, that cluster microphones near the centre for high frequency performance and distribute microphones far from the centre for low frequency performance (Dougherty, 1998). The corresponding numerically evaluated beamformer outputs are presented in Figures 3(b), 3(e) and 3(h) and the experimentally measured beamformer outputs in Figures 3(c), 3(f) and 3(i). By comparing the numerically and experimentally obtained beamformer maps at 1 kHz, it can be seen that the main lobe of the experimental map is slightly distorted in the x-direction and that there exists a secondary source at approximately $x = 250$ mm, $y = 450$ mm. Based on the corresponding numerical output, this is likely to be a reflected source from the polyurethane foam that was used to shield the rear of the speaker from hard-wall reflections. Despite the likely reflected source, the MLW values are comparable. The MLWs of the numerical and experimental beamformer maps at $f = 2$ kHz and 5 kHz show excellent agreement. In addition, the speaker cone diameter is a sufficiently large acoustic source, such that at higher frequencies the source location cannot be regarded as a point source. This emphasises the source location and main lobe estimation capability of an array designed using the iterative microphone removal method. The disparity in sidelobe levels may be due to reflective surfaces or errors in microphone estimation that are exacerbated during beamforming calculations at higher frequencies.

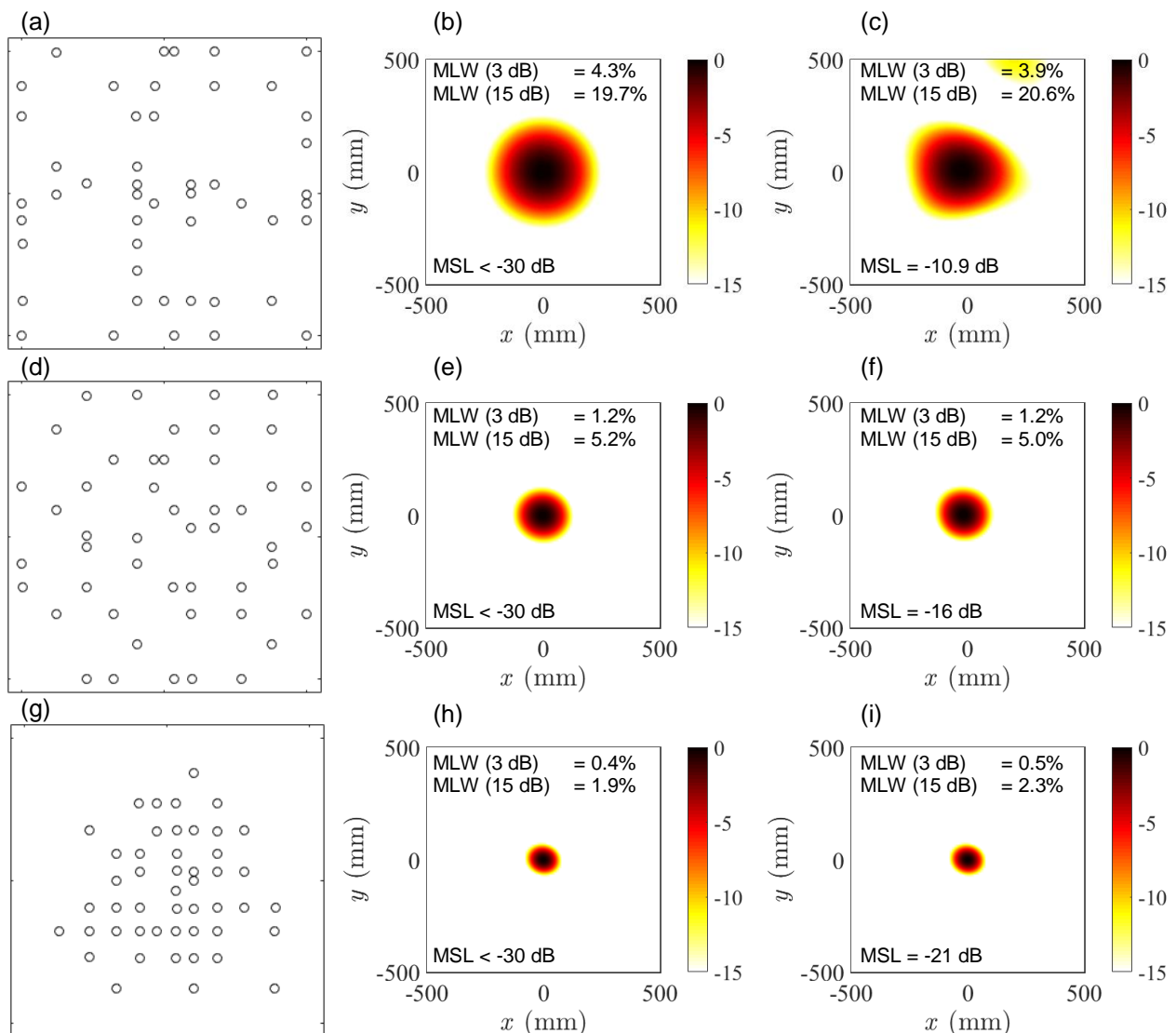


Figure 3: Single-frequency centred design arrays at (a) 1 kHz, (d) 2 kHz and (g) 5 kHz. Numerically obtained Y-values are presented in (b) 1 kHz, (e) 2 kHz and (h) 5 kHz and the experimentally obtained Y-values in (c) 1 kHz, (f) 2 kHz and (i) 5 kHz.

The multi-frequency array designed for an acoustic source at the scanning grid origin ($x = y = 0$ mm) using $f_{\min} = 2$ kHz and $f_{\max} = 8$ kHz and $f_s = 10$ is presented in Figure 4(a). The array design possesses microphones that spread over the majority of the array plane and also some microphones clustered near the centre, providing a balanced performance between f_{\min} and f_{\max} . At $f = 2$ kHz, the numerical main lobe size (shown in Figure 4(b)) is the same, with the experimental result (Figure 4(c)) displaying some distortion. Both maps do not possess any sidelobes within -15 dB of the main lobe. At $f = 4$ kHz, the numerical and experimental beamformer outputs agree well, as observed by comparing Figures 4(d) and 4(e), respectively. At $f = 6$ kHz, the experimentally obtained map (Figure 4(g)) displays some sidelobes (and/or reflected sources) yet the MLW is very similar to the numerical result shown in Figure 4(f). It should be noted that the speaker signal amplitude at 6 kHz was approximately 10 dB less than at the other frequencies, which may also contribute to the higher relative sidelobe magnitude. The main lobe agrees well with the numerical result nonetheless.

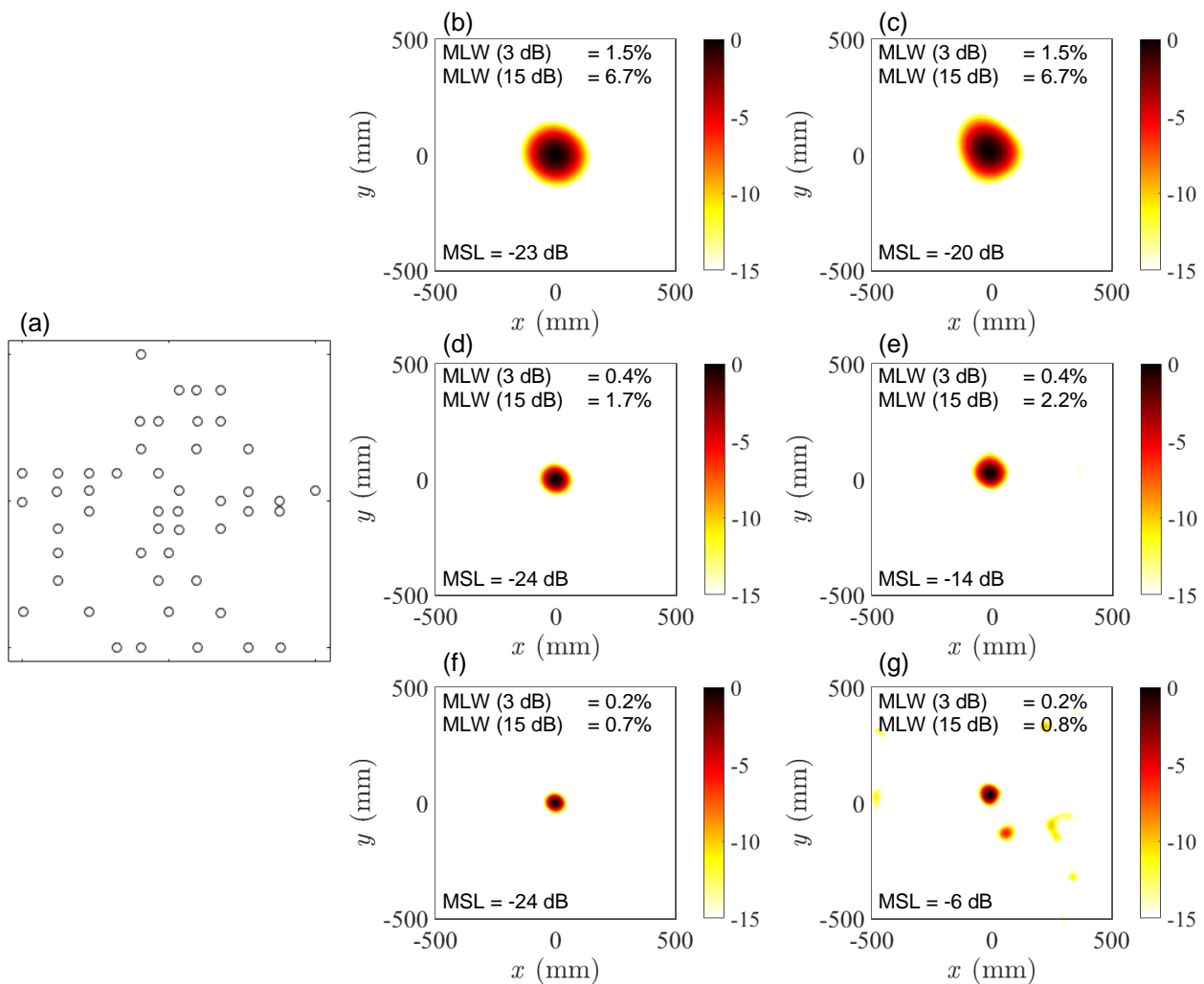


Figure 4: (a) Multi-frequency centred design array for $f_{\min} = 2$ kHz and $f_{\max} = 8$ kHz and $f_s = 10$. Numerically obtained Y-values are presented in (b) 2 kHz, (d) 4 kHz and (f) 6 kHz and the experimentally obtained Y-values in (c) 2 kHz, (e) 4 kHz and (g) 6 kHz.

Overall, it can be observed that the multi-frequency array design performs well for the investigated frequencies here; the sidelobe levels are low (or non-existent within a -15 dB threshold) and the main lobes are near-circular (little or no distortion).

5.2 Non-Centred Design Arrays

Arrays are designed by simulating a source that is located at $x = 200$ mm, $y = 0$ mm, to test the iterative microphone removal method's capability of source location. Single-frequency non-centred arrays are presented in Figures 5(a), 5(d) and 5(g) for $f = 1$ kHz, 2 kHz and 5 kHz, respectively. Each of the array possesses a greater distribution of microphones on the right-side of the array to improve the capability of locating a source at $x = 200$ mm. The arrays are also sparsely spaced for the $f = 1$ kHz array (analogous to Figure 3(a)) and become more densely spaced with increasing frequency. The numerical and experimental results in Figures 5(b) and 5(c) show a similar disparity to the $f = 1$ kHz results in Figures 3(b) and 3(c), in that the experimentally obtained 1 kHz main lobe possesses some distortion and a reflected source and/or sidelobe within the -15 dB threshold. The numerical and experimental results at $f = 2$ kHz and 5 kHz show good agreement with similar main lobe sizes and little distortion.

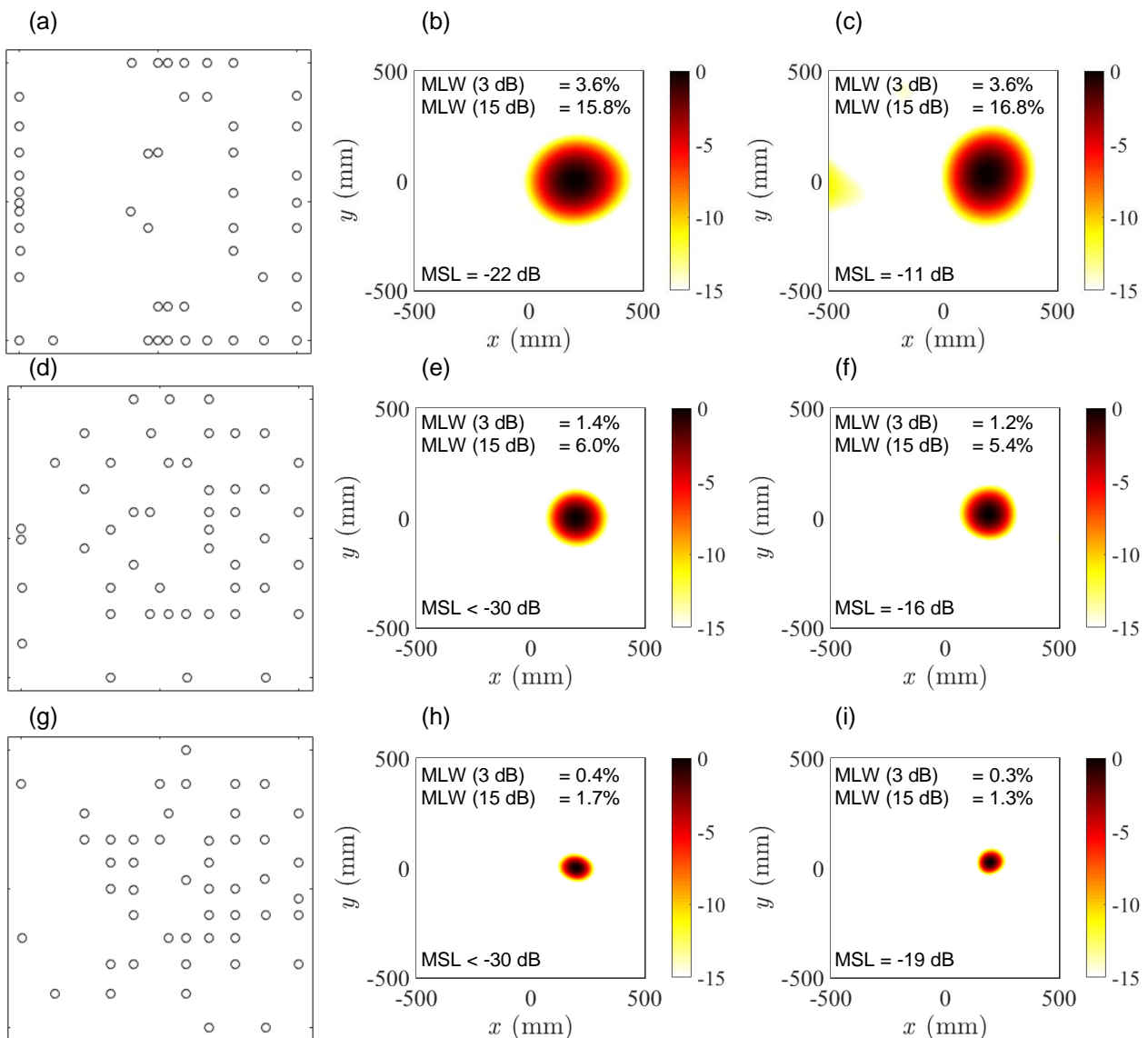


Figure 5: Single-frequency non-centred design arrays at (a) 1 kHz, (d) 2 kHz and (g) 5 kHz. Numerically obtained Y-values are presented in (b) 1 kHz, (e) 2 kHz and (h) 5 kHz and the experimentally obtained Y-values in (c) 1 kHz, (f) 2 kHz and (i) 5 kHz.

The multi-frequency array designed for an acoustic source away from scanning grid origin ($x = 200 \text{ mm}$, $y = 0 \text{ mm}$) using $f_{\min} = 2 \text{ kHz}$ and $f_{\max} = 8 \text{ kHz}$ and $f_s = 10$ is presented in Figure 6(a). A distribution of microphones are placed on the upper and right-side boundary of the array area, bearing similarity with the $f = 1 \text{ kHz}$ single-frequency non-centred array shown in Figure 5(a). The microphones clustered near the centre act to improve the source map at higher frequencies. At $f = 1 \text{ kHz}$, the numerical and experimentally obtained maps (Figures 6(b) and 6(c) respectively) show similar MLW values, with the experimental result showing some x-direction lobe distortion. Excellent agreement with MSL and MLW is observed at $f = 4 \text{ kHz}$ as observed by comparing Figures 6(d) and 6(e). At $f = 6 \text{ kHz}$ the experimental result shown in Figure 6(g) displays some lobe distortion and sidelobes compared to the numerical result in Figure 6(f), yet as discussed in Section 5.1, the signal-to-noise ratio at this frequency was diminished.

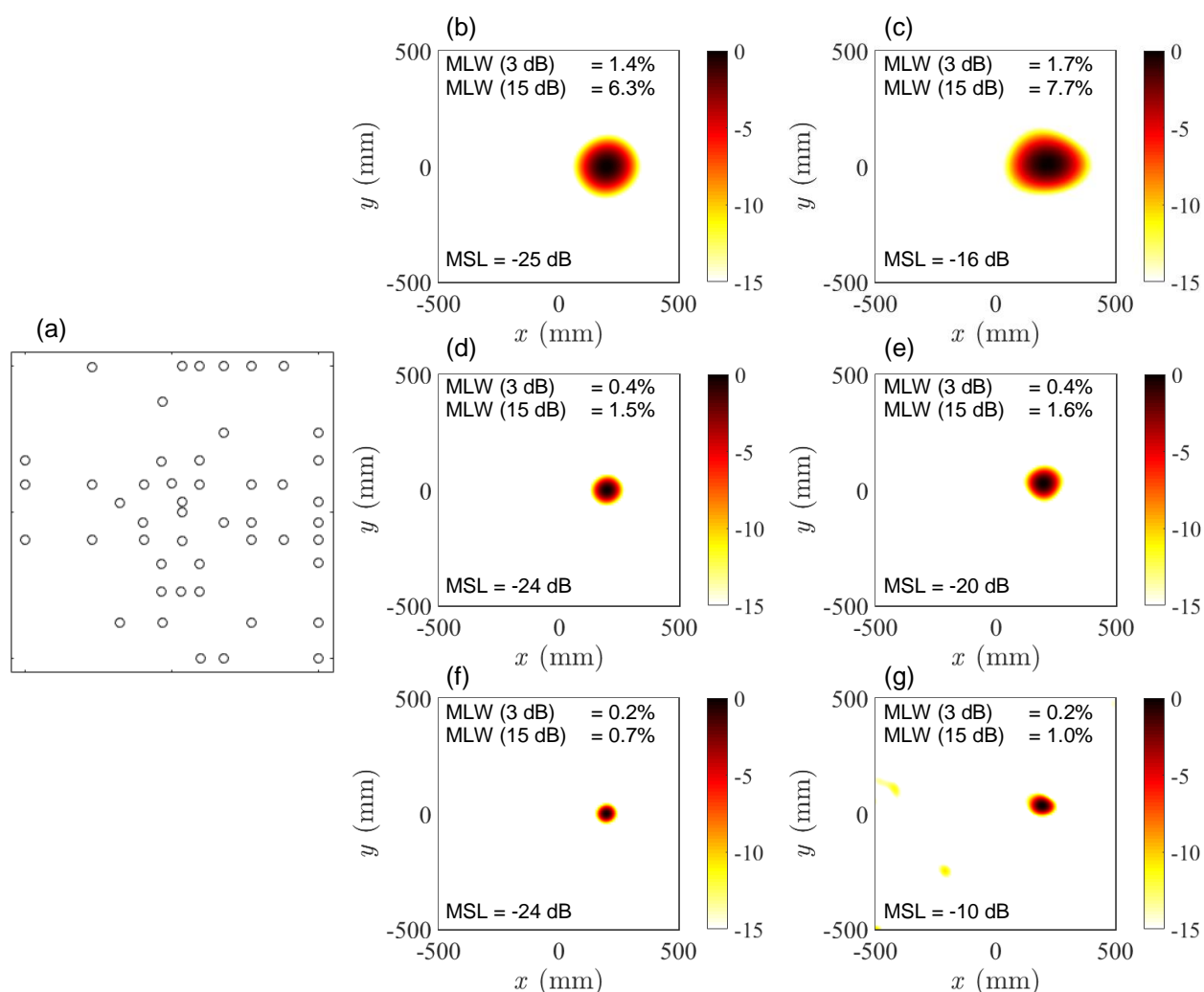


Figure 6: (a) Multi-frequency non-centred design array for $f_{\min} = 2 \text{ kHz}$ and $f_{\max} = 8 \text{ kHz}$ and $f_s = 10$. Numerically obtained Y-values are presented in (b) 2 kHz, (d) 4 kHz and (f) 6 kHz and the experimentally obtained Y-values in (c) 2 kHz, (e) 4 kHz and (g) 6 kHz.

6 REMARKS

It should be noted that the process of interchanging microphones at the rear of the panel is simple and convenient. The microphones of the new and previous arrays are interchanged via microphone number (not coordinates: e.g., the microphone placed in slot 36 is moved to slot 148). Each array was arranged within 10 minutes by a single person. A much faster time could be achieved with the aid of a helper. Furthermore, each unique array does not require additional calibration, as the uncertainty of the microphone locations of the grid will be the same per array design. The initial array stencil can be varied into any shape or size, such as a circular pattern

or even a densely spaced spiral pattern, based on its expected use (eg: small-scale anechoic wind tunnels up to large-scale industrial noise or full-scale aircraft noise measurements). This is a unique concept of acoustic beamforming that is versatile, fast to assemble and can be designed specifically for expected source frequencies and source location that is difficult to achieve with a fixed installation multi-purpose array such as a spiral-based array (Arcondoulis and Liu, 2018).

7 CONCLUSIONS

An iterative microphone removal method, previously presented by the current authors, was used to create new 48-channel array designs, using single-frequency and multi-frequency methods and sources located away from the scanning grid origin. These arrays were experimentally tested in a non-anechoic environment using an interchangeable 169-channel stencil and a small speaker that revealed good agreement with the numerically generated maps, despite potential errors due to the reflective environment. The centred and non-centred arrays experimentally locate the acoustic sources with comparable main lobe sizes to the numerical beamformer maps. The iterative microphone removal method has shown to be a quick and convenient method to beamform sources of specific frequencies at specific locations. To formally quantify these array capabilities, further testing is required in an anechoic environment. Thus future tests will be conducted in an anechoic facility, with a greater number of source locations and thus specific array designs. Different initial array stencils will be simulated and manufactured for specific aeroacoustic noise sources.

ACKNOWLEDGEMENTS

This research was supported by the National Natural Science Foundation of China (Grant No. 11772146) and the Science and Technology Innovation Council of Shenzhen (Grant No. JCYJ20170817110605193).

REFERENCES

- Arcondoulis, E., Doolan, C., Brooks, L., and Zander, A., 2011, "A modification to logarithmic spiral beamforming arrays for aeroacoustic applications," *Proceedings of the 17th AIAA/CEAS Aeroacoustics Conference*, AIAA Paper 2011-2720 (2011).
- Arcondoulis, E., and Liu, Y., 2018, "Acoustic beamforming array design using an iterative microphone removal method." *Proceedings of the 24th AIAA/CEAS Aeroacoustics Conference*, AIAA Paper 2018-2807 (2018).
- Brooks, T. F., and Humphreys, W. M., 2006, "A deconvolution approach for the mapping of acoustic sources (DAMAS) determined from phased microphone arrays," *Journal of Sound and Vibration*, Vol. 294, No. 4, 2006, pp. 856–879.
- Bjelić, M., Stanojevic, M., Šumarac Pavlovic, D., and Mijic, M., 2017, "Microphone array geometry optimization for traffic noise analysis," *The Journal of the Acoustical Society of America*, Vol. 141, No. 5, 2017, pp. 3101–3104.
- Dobrzynski, W., Chow, L. C., Smith, M., Boillot, A., Dereure, O., and Molin, N., 2010, "Experimental assessment of low noise landing gear component design," *International Journal of Aeroacoustics*, Vol. 9, No. 6, 2010, pp. 763–786.
- Dougherty, R.P., "Spiral-shaped array for broadband imaging", US Patent, No. 5838284.
- Luesutthiviboon, S., Malgoezar, A., Snellen, M., Sijtsma, P., and Simons, D., 2018, "Improving source discrimination performance by using an optimized acoustic array and adaptive high-resolution CLEAN-SC beamforming." In *7th Berlin Beamforming Conference*, Paper No. BeBeC-2018-D7 (2018).
- Ma, W., and Liu, X., 2018, "Phased microphone array for sound source localization with deep learning", arXiv preprint arXiv:1802.04479.
- Malgoezar, A., Snellen, M., Sijtsma, P., and Simons, D., 2016, "Improving beamforming by optimization of acoustic array microphone positions," *Proceedings of the 6th Berlin Beamforming Conference*, Paper No. BeBeC-2016-D5 (2016).
- Prime, Z., and Doolan, C., 2013, "A comparison of popular beamforming arrays", *Australian Acoustical Society*, AAS2013, Victor Harbor, Vol 1. (2013) Paper No. 5.
- Sijtsma, P., 1997, "Optimum arrangements in a planar microphone array," *First CEASASC Workshop: Wind Tunnel Testing in Aeroacoustics*, DNW, Vol. 5, 1997, p. 6.
- Sijtsma, P., 2010, *Phased array beamforming applied to wind tunnel and fly-over tests*, SAE Technical Paper, 2010.
- Underbrink, J. R., 2002, "Aeroacoustic phased array testing in low speed wind tunnels," *Aeroacoustic Measurements*, Springer, 2002, pp. 98–217.